Int. J. Solids Structures Vol. 29, No. 7, pp. 801–824, 1992
Printed in Great Britain.

0020–7683/92 $5.00 + .00

NON-NORMALITY AND BIFURCATION IN A COMPRESSIBLE PRESSURE-SENSITIVE CIRCULAR CYLINDER UNDER AXISYMMETRIC TENSION AND COMPRESSION

K. T. CHAU
Department of Civil Engineering, McCormick School of Engineering and Applied Science, Northwestern University, Evanston, IL 60208-3109, U.S.A.

(*Received* 26 *February* 1991; *in revised form* 2 *June* 1991)

Abstract—This paper examines bifurcations, including diffuse bifurcation modes of deformation, such as necking, bulging and surface rumpling, and localized bifurcation modes, corresponding to the formation of shear bands, for a compressible pressure-sensitive circular cylinder under axisymmetric deformations. The analysis emphasizes the effects of non-normality, transverse anisotropy, and confining stress on the appearance of diffuse modes and their relationship to the onset of localization. In particular, introduction of transverse anisotropy and non-normality promotes not only localization but also geometric diffuse modes under compression. In addition, constant compressive confining stress promotes diffuse modes under compression but hinders them under tension. For the surface rumpling mode (short wavelength limit of diffuse mode), both anisotropy and compressive lateral stress favor pre-peak bifurcations; in-plane compressibility promotes pre-peak bifurcations under compression but retards them under tension. Numerical solutions of the eigenvalue equation for the elliptic complex regime demonstrate that the earliest bifurcation available is the diffuse necking mode under tension. However, unexpectedly, some geometric diffuse modes with finite wave number, instead of the bulging mode, become the first possible bifurcation under compression. The possible angle of localization that may be triggered by such diffuse modes is about the same as those predicted by shear band analysis. Consequently, such diffuse eigenmodes may trigger localization in the vicinity of peak applied stress.

1. INTRODUCTION

Bifurcations, such as diffuse geometric modes and localized shear band modes, are often-observed phenomena in material testing. Therefore, a detailed bifurcation analysis, which includes diffuse modes and the relation of their appearance to the onset of localization, may provide considerable insight into the failure process.

Since the most commonly employed testing configuration, particularly for geomaterials, uses circular cylindrical specimens, we examine axisymmetric bifurcations from states of uniform compression or extension of circular cylinders. Although the constitutive relation we employ is general, our emphasis is on applications to geomaterials, especially brittle rocks.

In the axisymmetric compression test, localization of deformation is often related to the final failure mode in rocks. The analysis of strain localization from axisymmetric deformation states by Rudnicki and Rice (1975) suggests that localization in a specimen under compression appears relatively late in the post-peak applied stress regime. Experimental evidence is, however, not definite in supporting whether the development of strain localization occurs preceding or after peak applied stress. In particular, although there are some experimental observations [e.g. Rummel and Fairhurst (1970); Wawersik and Fairhurst (1970); Wawersik and Brace (1971); Fredrich *et al.* (1989)] that support the prediction by Rudnicki and Rice (1975), more frequently, localization is observed preceding peak applied stress [see summary of experimental observations by Santarelli and Brown (1989)]. Even though Rudnicki (1977) concluded that stress-induced anisotropy may cause some reduction in the amount of post-peak deformation predicted for localization, extreme values of material parameters are necessary to obtain pre-peak localization. In this study, we attempt to relate the strain localization observed preceding peak applied stress to the diffuse modes available in the hardening stage of the stress–strain curve. In particular, we

investigate the hypothesis that diffuse geometric modes trigger non-homogeneous deformation and, eventually, lead to pre-peak localization of deformation.

More specifically, this paper considers bifurcations of a circular cylinder deformed in axisymmetric tension or compression. The ends of the cylinder are loaded by a prescribed velocity with no shear traction; and a constant lateral stress is applied with zero shear traction on the sides of the cylinder. An initial state of homogeneous deformation is always a solution to governing equations and we investigate the conditions for which a bifurcated state of non-uniform deformation is also possible under the same boundary conditions. We consider both diffuse bifurcation modes, such as necking, bulging and surface rumpling, and localized bifurcation modes, corresponding to the loss of ellipticity or the shear band modes. An incrementally linear constitutive model, including transverse anisotropy and non-normality, introduced by Rudnicki (1977) is employed in this study. In particular, the direction of the inelastic strain increment described by the model does not, in general, coincide with the normal to the yield surface in the stress space; and transverse anisotropy is introduced by assuming different longitudinal and transverse shear moduli. The consequences due to such material behaviors on the appearance of diffuse modes are emphasized; and the possible connection of diffuse mode to the onset of localization is examined.

The present paper is a continuation of the works by Cheng *et al.* (1971), Hutchinson and Miles (1974), Rudnicki (1977) and Miles and Nuwayhid (1985) and provides an analogous study of the plane strain counterpart by Chau and Rudnicki (1990). Elaborating upon the work of Miles (1971) and Cheng *et al.* (1971), Hutchinson and Miles (1974) extended the analysis of necking bifurcation of an incompressible cylinder under uniaxial tension to include transverse anisotropy. No non-normality is incorporated in the above studies. Miles and Nuwayhid (1985) further extend the analysis to include compressibility but do not consider anisotropy. Because the constitutive law used by Miles and Nuwayhid (1985) is written in terms of the Jaumann rate of Cauchy stress and the rate-of-deformation, it does not satisfy precise normality in work-conjugate variables. However, this relation does not allow for the type of non-normality typical of brittle rocks. Therefore, the role of non-normality in bifurcation analysis under axisymmetric deformation is examined here.

Vardoulakis (1983) carried out a bifurcation analysis, which is similar to that considered here, for a rigid-plastic circular cylinder with non-associated flow rule and plastic dilatation. The constitutive law used by Vardoulakis (1983) can be interpreted as a special case of Rudnicki's (1977) relation which is employed in this paper. However, he limits consideration to parameters typical of a particular dry sand. Furthermore, the effect of non-normality and anisotropy on geometric diffuse modes is not fully explored.

2. CONSTITUTIVE RELATION

We consider a circular cylinder of radius a and length L under axisymmetric deformations. The current configuration is adopted as a reference and the subsequent deformation of the material is characterized by the following time- and rate-independent constitutive relation (Rudnicki, 1977):

$$D_{zz} = \frac{1}{E}\left[\overset{\nabla}{\sigma}_{zz} - \frac{r^*}{2}(\overset{\nabla}{\sigma}_{rr} + \overset{\nabla}{\sigma}_{\theta\theta})\right],$$

$$D_{\alpha\beta} = -\nu D_{zz}\delta_{\alpha\beta} + \frac{1}{2G_t}[\overset{\nabla}{\sigma}_{\alpha\beta} - \tfrac{1}{2}\delta_{\alpha\beta}(\overset{\nabla}{\sigma}_{rr} + \overset{\nabla}{\sigma}_{\theta\theta})] + \delta_{\alpha\beta}\left(\frac{\overset{\nabla}{\sigma}_{rr} + \overset{\nabla}{\sigma}_{\theta\theta}}{9K}\right),$$

$$D_{z\alpha} = \frac{\overset{\nabla}{\sigma}_{z\alpha}}{2G_t}, \quad (\alpha, \beta = r, \theta) \tag{1}$$

where (r, θ, z) are cylindrical polar coordinates, $\boldsymbol{\sigma}$ is the Cauchy stress, the superposed ∇ denotes the Jaumann or co-rotational rate (Prager, 1961), and $\mathbf{D}$ is the rate of deformation tensor.

As discussed by Rudnicki (1977), E is the instantaneous tangent modulus, that is, the slope of the axial stress–strain curve at fixed confining stress. In particular, E decreases with deformation, equals zero at peak applied stress, and becomes negative for softening regime. The axial straining is inhibited by the lateral stress rate by a factor of r^*. Thus, the pressure sensitivity of the material is described by this parameter r^*.

The second of (1) can be rearranged as

$$\tfrac{1}{2}(D_{rr}+D_{\theta\theta}) = -\nu D_{zz}+\frac{1}{9K}(\overset{\nabla}{\sigma}_{rr}+\overset{\nabla}{\sigma}_{\theta\theta}),$$

$$D_{rr}-D_{\theta\theta} = \frac{1}{2G_t}(\overset{\nabla}{\sigma}_{rr}-\overset{\nabla}{\sigma}_{\theta\theta}), \tag{2}$$

in order to interpret other material parameters. For constant lateral confining stress, the effective Poisson's ratio ν is the slope of the lateral strain versus axial strain curve. In general, $\nu > 1/2$ for dilatant materials. In particular, for brittle rocks, a typical range of 1.0–2.4 near the peak applied stress is observed under axisymmetric compressions (Rudnicki, 1977). G_t and G_l are the incremental transverse shear and longitudinal shear moduli. The in-plane bulk modulus is denoted by K.

As mentioned by Rudnicki (1977), it is difficult to interpret r^* and K from the existing experimental data. Therefore, it will be helpful to compare (1) and the axisymmetric form of the isotropic constitutive law introduced by Rudnicki and Rice (1975). As expected, E is found to be proportional to the plastic hardening modulus h while K is on the order of elastic modulus. If the plastic hardening modulus is negligible compared with the elastic moduli, then r^* and 2ν are found to be

$$r^* = (\delta-2\mu/\sqrt{3})/(\delta+\mu/\sqrt{3}),$$
$$2\nu = (\delta-2\beta/\sqrt{3})/(\delta+\beta/\sqrt{3}), \tag{3}$$

where $\delta = \text{sign}\,(\sigma_{zz}-\sigma_{rr})$, μ is a friction coefficient and β is the dilatancy factor (Rudnicki and Rice, 1975).

As mentioned by Rudnicki and Rice (1975), the typical range for μ is 0.4–0.9 and for β is 0.2–0.4 for brittle rocks. Thus, with these values (3) gives $2\nu \geqslant r^*$ for tensile loads and $2\nu \leqslant r^*$ for compressive loads. More specifically, ν ranges from 0.70–0.95 for compression and 0.22–0.35 for tension while r^* ranges from 1.90–4.25 for compression and 0–0.44 for tension (μ must be less than $\sqrt{3}/2$ in order for r^* to be positive in the case of tension). Equation (3) also suggests that r^* and ν can be identified as the pressure-sensitivity and the dilatancy factors respectively for the axisymmetric case. Furthermore, since $\beta = \mu$ implies that the direction of inelastic strain increment coincides with the normal to the yield surface,

$$r^* = 2\nu, \tag{4}$$

implies normality. However, precise normality of work-conjugate variables requires that σ in (1) be replaced by Kirchhoff stress τ ($=\sigma\,(\rho/\rho_0)$, where ρ and ρ_0 are the densities of the current and reference configurations) which is work-conjugate to $\mathbf{D}$ (Hill, 1968, 1978).

The form of the constitutive relation considered by Hutchinson and Miles (1974) can be recovered by specialization of (1), in particular, by considering the incompressible ($K \to \infty$ and $\nu = 1/2$) and pressure insensitive ($r^* = 1$) limits of (1). Similarly, setting $r^* = 2\nu$ and $G_t = G_l$ in (1) recovers the constitutive model by Miles and Nuwayhid (1985). Furthermore, the rigid-granular dilatant material considered by Vardoulakis (1983) can also be recovered by assuming that E, K, r^* and ν are some specific functions of Cauchy stress, the Jaumann rate of Cauchy stress and the rate of deformation. Such constitutive assumptions are, in general, too specific for rocks. In particular, the incremental parameters can depend on the current stress or strain state but not necessarily in the way suggested by Vardoulakis (1983).

The maximum load point can be evaluated by setting

$$\dot{t}_{zz} = 0, \quad \dot{t}_{rr} = 0, \quad \dot{t}_{\theta\theta} = 0, \tag{5}$$

where $\dot{\mathbf{t}}$ is the nominal stress rate. The rate of deformation tensor is defined as

$$\mathbf{D} = \tfrac{1}{2}(\mathbf{L} + \mathbf{L}^{\mathrm{T}}), \tag{6}$$

where the superscript $(\ )^{\mathrm{T}}$ denotes the transpose of $(\ )$. For axisymmetric deformations, the velocity gradient tensor is given by

$$\mathbf{L}^{\mathrm{T}} = \nabla \mathbf{v} = \frac{\partial v_r}{\partial r}\mathbf{e}_r\mathbf{e}_r + \frac{\partial v_z}{\partial r}\mathbf{e}_r\mathbf{e}_z + \frac{\partial v_r}{\partial z}\mathbf{e}_z\mathbf{e}_r + \frac{\partial v_z}{\partial z}\mathbf{e}_z\mathbf{e}_z + \frac{v_r}{r}\mathbf{e}_\theta\mathbf{e}_\theta, \tag{7}$$

where $\mathbf{v}$ is the velocity vector and $\mathbf{e}_r$, $\mathbf{e}_\theta$ and $\mathbf{e}_z$ are the base vectors to the cylindrical coordinate system. Substitution of (7) into (6) gives:

$$D_{zz} = \frac{\partial v_z}{\partial z}, \quad D_{rr} = \frac{\partial v_r}{\partial r}, \quad D_{\theta\theta} = \frac{v_r}{r}, \quad D_{rz} = \frac{1}{2}\left(\frac{\partial v_r}{\partial z} + \frac{\partial v_z}{\partial r}\right). \tag{8}$$

In addition, the material time rate and the Jaumann rate of Cauchy stress are related as

$$\overset{\nabla}{\boldsymbol{\sigma}} = \dot{\boldsymbol{\sigma}} - \mathbf{W}\cdot\boldsymbol{\sigma} + \boldsymbol{\sigma}\cdot\mathbf{W}, \tag{9}$$

where $\mathbf{W} = (\mathbf{L} - \mathbf{L}^{\mathrm{T}})/2$. More specifically, under axisymmetric stresses (only σ_{rr}, $\sigma_{\theta\theta}$ and σ_{zz} are non-zero), substitution of (7) into (9) yields

$$\overset{\nabla}{\sigma}_{rr} = \dot{\sigma}_{rr}, \quad \overset{\nabla}{\sigma}_{\theta\theta} = \dot{\sigma}_{\theta\theta}, \quad \overset{\nabla}{\sigma}_{zz} = \dot{\sigma}_{zz}, \quad \overset{\nabla}{\sigma}_{rz} = \dot{\sigma}_{rz} - \frac{1}{2}\left(\frac{\partial v_r}{\partial z} - \frac{\partial v_z}{\partial r}\right)(\sigma_{zz} - \sigma_{rr}). \tag{10}$$

Furthermore, since the current configuration is adopted as reference, that is $\det(\mathbf{F}) = 1$ and $\mathbf{F} = \mathbf{I}$ where $\mathbf{F}$ is the deformation gradient tensor and $\mathbf{I}$ is the second order unit tensor, the nominal and Cauchy stress rates are related as:

$$\dot{\mathbf{t}} = \dot{\boldsymbol{\sigma}} + \boldsymbol{\sigma}\,\mathrm{tr}(\mathbf{D}) - \mathbf{L}\cdot\boldsymbol{\sigma}, \tag{11}$$

where $\mathrm{tr}(\mathbf{D})$ is the trace of $\mathbf{D}$. Substitution of (7), (8) and (10) into (11) yields

$$\begin{aligned}
\dot{t}_{zz} &= \overset{\nabla}{\sigma}_{zz} + \sigma_{zz}\left(\frac{\partial v_r}{\partial r} + \frac{v_r}{r}\right), \quad \dot{t}_{rr} = \overset{\nabla}{\sigma}_{rr} + \sigma_{rr}\left(\frac{v_r}{r} + \frac{\partial v_z}{\partial z}\right),\\
\dot{t}_{zr} &= \overset{\nabla}{\sigma}_{zr} - \sigma_{rr}\frac{\partial v_z}{\partial r} + \tfrac{1}{2}(\sigma_{zz} - \sigma_{rr})\left(\frac{\partial v_r}{\partial z} - \frac{\partial v_z}{\partial r}\right),\\
\dot{t}_{rz} &= \overset{\nabla}{\sigma}_{rz} - \sigma_{zz}\frac{\partial v_r}{\partial z} + \tfrac{1}{2}(\sigma_{zz} - \sigma_{rr})\left(\frac{\partial v_r}{\partial z} - \frac{\partial v_z}{\partial r}\right),\\
\dot{t}_{\theta\theta} &= \overset{\nabla}{\sigma}_{\theta\theta} + \sigma_{\theta\theta}\left(\frac{\partial v_r}{\partial r} + \frac{\partial v_z}{\partial z}\right).
\end{aligned} \tag{12}$$

Then, eqns (1) can be rewritten in terms of $\dot{\mathbf{t}}$ then (5) is used to yield three simultaneous equations for three components of the rate of deformation tensor (D_{rr}, $D_{\theta\theta}$ and D_{zz}). The condition for non-trivial $\mathbf{D}$ leads to the following expression for the stress at maximum load

$$\sigma_{zz}^{\max} = \frac{E}{2\nu}\left[\frac{1+\sigma_{rr}[2/9K - r^*(1-\nu)/E]}{1+2\sigma_{rr}/9K\nu}\right], \tag{13}$$

where we have used $\sigma_{rr} = \sigma_{\theta\theta}$ as appropriate for a homogeneous axisymmetric state. As observed in plane strain deformation (Chau and Rudnicki, 1990), $\sigma_{zz}^{\max}$ differs from the tangent modulus E unless the solid is incompressible ($K \to \infty$ and $\nu = 1/2$) and σ_{rr} is zero. It will be shown in Section 5 that $\sigma_{zz}^{\max}$ appears naturally as the first term of eigenstress for the long wavelength diffuse mode.

For a smooth yield surface, G_l and G_t are essentially elastic moduli. However, if a yield surface vertex is formed at the current stress point, as suggested in models for metal polycrystalline aggregates based on single crystal plasticity (Hill, 1967; Hutchinson, 1970; Lin, 1971), G_l and G_t may be significantly reduced from the elastic values. Rudnicki and Rice (1975) also argued that formation of a yield surface vertex is possible in brittle rocks due to frictional sliding on fissure surfaces. As suggested by Rudnicki (1977), this yield vertex effect may be included into (1) by simply regarding G_t and G_l as the vertex reduced shear moduli. Such an interpretation of G_t and G_l plays an essential role in understanding the shear band bifurcation mode (Rudnicki and Rice, 1975; Rudnicki, 1977).

As discussed by Needleman (1979) and Chau and Rudnicki (1990), for solids that do not satisfy plastic normality, Hill's (1958, 1961a, 1978) general theory of bifurcation and uniqueness, which is based on the idea of "linear comparison solid", is not applicable. Consequently, (1) can only provide the upper bound of the bifurcation stress in the sense of Raniecki and Bruhns (1981).

3. GOVERNING EQUATIONS

This section closely follows Miles and Nuwayhid (1985) and the mathematical detail should be referred to these authors. For a finite cylinder of radius a and length L, a cylindrical polar coordinate system (r, θ, z), with origin resting on the bottom of the cylinder and z-axis coincident with the axis of symmetry, is used. The ends ($z = 0, L$) are loaded by a prescribed velocity in the z-direction in such a way that shear traction vanishes. A constant lateral stress is applied in the r-direction such that no shear traction is induced on $r = a$. The circular cylinder is homogeneously deformed in the current state and a further homogeneous deformation is always a possible solution for the next increment of deformation. If there exists an alternative solution for the next increment of deformation, bifurcation occurs. The difference between the bifurcation and the homogeneous solution is denoted by the superscript *. More specifically, we are seeking a non-trivial solution for the difference in incremental stress rates $\dot{\sigma}_{rr}^*$ and $\dot{\sigma}_{rz}^*$ and the velocity field v_r^* and v_z^*.

The boundary conditions governing the difference in incremental solutions are then

$$v_z^* = 0, \quad i_{zr}^* = \dot{\sigma}_{rz}^* - \sigma_{rr}\frac{\partial v_z^*}{\partial r} = 0, \quad \text{on} \quad z = 0, L, \tag{14}$$

and

$$i_{rr}^* = \dot{\sigma}_{rr}^* + \sigma_{rr}\left(\frac{v_r^*}{r} + \frac{\partial v_z^*}{\partial z}\right) = 0,$$

$$i_{rz}^* = \dot{\sigma}_{rz}^* - \sigma_{zz}\frac{\partial v_r^*}{\partial z} = 0, \tag{15}$$

on $r = a$. Note that the "follower type" of confining stress, which acts always normal on the deforming boundary of the cylinder, considered by Cheng *et al.* (1971) and Vardoulakis (1983) can be recovered simply by setting $\sigma_{rr} = 0$ in the first of (15).

Continued equilibrium of both incremental solutions can be written in terms of Cauchy stress rate as follows

$$\frac{\partial \dot{\sigma}_{rr}^*}{\partial r} + \frac{\partial \dot{\sigma}_{zr}^*}{\partial z} + \frac{\dot{\sigma}_{rr}^* - \dot{\sigma}_{\theta\theta}^*}{r} + \left(\frac{\sigma_{rr} - \sigma_{\theta\theta}}{r}\right)\left(\frac{\partial v_r^*}{\partial r} + \frac{\partial v_z^*}{\partial z}\right) = 0,$$

$$\frac{1}{r}\frac{\partial}{\partial r}(r\dot{\sigma}_{rz}^*) + \frac{\partial \dot{\sigma}_{zz}^*}{\partial z} = 0, \tag{16}$$

with $\dot{\sigma}_{r\theta}$ and $\dot{\sigma}_{\theta z}$ being zero.

For compressible solids, the stream function employed by Hutchinson and Miles (1974) does not exist. However, since σ_{rr} equals $\sigma_{\theta\theta}$ for the homogeneous primary state, a stress rate potential $\chi(r, z)$ can be defined such that (Miles and Nuwayhid, 1985)

$$\dot{\sigma}_{zz} = \frac{1}{r}\frac{\partial}{\partial r}\left(r\frac{\partial \chi}{\partial r}\right), \quad \dot{\sigma}_{rz} = -\frac{\partial^2 \chi}{\partial r\, \partial z}. \tag{17}$$

A similar stress potential has been used by Love (1927) in calculating the stress distribution in an isotropic elastic circular cylinder; Elliott (1948) further showed that Love's stress function can be used to solve elastic problems in transversely isotropic solids. By combining (1), (10) and (17), the velocity components, v_r and v_z, are found to be

$$\frac{1}{r}\frac{\partial}{\partial r}(rv_r) = \frac{1}{\sigma_m}\left[\left(\frac{9Kr^*v + 2E}{9Kv}\right)\frac{\partial^2 \chi}{\partial z^2} - L_1\chi\right],$$

$$\frac{\partial v_z}{\partial z} = \frac{1}{2v\sigma_m}\left[\left(\frac{4G_t + 9K}{9K}\right)L_1\chi - r^*\frac{\partial^2 \chi}{\partial z^2}\right], \tag{18}$$

where

$$\sigma_m = [E(4G_t + 9K) + 18KG_t r^* v]/(18Kv) \quad \text{and} \quad L_1(\ \ ) = \frac{1}{r}\frac{\partial}{\partial r}\left[r\frac{\partial(\ \ )}{\partial r}\right].$$

Note that σ_m has the interpretation as the stress at maximum load for the same material under plane strain deformation. More specifically, if $D_{22} = 0$ (or equivalently $D_{11} = 0$) in the Cartesian form of (1) with the z-axis replaced by x_3-axis, then $\overset{\nabla}{\sigma}_{22}$ (or equivalently $\overset{\nabla}{\sigma}_{11}$) can be eliminated to give a plane strain version of (1). By using the conditions for a load maximum given by Chau and Rudnicki (1990), the stress at the maximum load point is found to be equal to σ_m given above. Similarly, the Cauchy stress rate, $\dot{\sigma}_{\theta\theta}$ and $\dot{\sigma}_{rr}$, can be obtained in terms of material parameters and the stress rate potential $\chi(r, z)$:

$$\dot{\sigma}_{\theta\theta} = \frac{9Kv}{9Kr^*v + 2E}\left[\sigma_m\frac{v_r}{r} - \left(\sigma_m - \frac{E}{v}\right)\frac{\partial v_r}{\partial r} + \frac{1}{r}\frac{\partial}{\partial r}\left(r\frac{\partial \chi}{\partial r}\right)\right],$$

$$\dot{\sigma}_{rr} = \frac{9Kv}{9Kr^*v + 2E}\left[\frac{E}{2v}\left(\frac{\partial v_r}{\partial r} + \frac{v_r}{r}\right) + \frac{1}{r}\frac{\partial}{\partial r}\left(r\frac{\partial \chi}{\partial r}\right)\right] + G_t\left(\frac{\partial v_r}{\partial r} - \frac{v_r}{r}\right). \tag{19}$$

Furthermore, by combining the last of (1), (8) and (10), the following expression is obtained

$$\frac{\dot{\sigma}_{rz}}{G_t} = \frac{\partial v_r}{\partial z}(1 + s) + \frac{\partial v_z}{\partial r}(1 - s), \tag{20}$$

with $s = (\sigma_{zz} - \sigma_{rr})/2G_t$. Finally, the second of (17) and (18) are substituted into (20) to yield the following governing equation for χ:

$$AL_1^2\chi + BL_1\frac{\partial^2\chi}{\partial z^2} + C\frac{\partial^4\chi}{\partial z^4} = 0. \tag{21}$$

The coefficients, A, B and C, are defined as

$$\begin{aligned} A &= (1-s)(4G_t+9K), \\ B &= E(4G_t+9K)/G_1 + 9K[2r^*vG_t/G_1 - (2v+r^*) + s(r^*-2v)], \\ C &= 2(1+s)(9Kr^*v+2E). \end{aligned} \tag{22}$$

In general, (21) can be elliptic, hyperbolic or parabolic depending on the coefficients A, B and C. Such classification of (21) is related to the classification of bifurcation regime, which will be considered next.

4. LOCALIZATION AND CLASSIFICATION OF REGIMES

The onset of strain localization in a narrow band with normal **g** is considered in this section. A more general treatment of shear band analysis has been given by Rice (1976). Geometrical compatibility requires the velocity increment to be continuous but permits a jump in the velocity gradient across the band (Hill, 1961b, 1962; Rice, 1976)

$$t^*_{\alpha,\beta} = c_\alpha g_\beta, \quad (\alpha,\beta = r,z) \tag{23}$$

where c_α are the components of jump and **g** is the normal to the incipient band.

Incremental equilibrium across the band gives

$$g_\beta t^*_{\beta\alpha} = 0, \quad (\alpha,\beta = r,z). \tag{24}$$

Equations (23) and (24) are the two basic conditions to be satisfied across the shear band. Substitution of (1) and (23) into (24) provides two simultaneous equations for c_r and c_z. For a non-trivial solution for velocity gradient jumps, the determinant of the coefficients for c_r and c_z have to vanish. This gives a 4th order algebraic equation

$$Ag_r^4 + Bg_r^2g_z^2 + Cg_z^4 = 0, \tag{25}$$

where A, B and C have been defined in (22).

Shear band bifurcation is possible only if a real value for the ratio g_r/g_z exists. Thus, the type of the governing equation for $\chi(r,z)$, (21) and (22), also determines the number of real roots for g_r/g_z. As discussed by Hill and Hutchinson (1975), the partial differential equation (21) is elliptic, parabolic or hyperbolic if there are zero, two or four real roots for (25) respectively [also see Hill (1979)].

The regimes for different behavior are summarized as:

Elliptic:

$$\frac{E}{G_1} > \frac{8(1-s^2)G_1 + 9K[2v+r^*+s(2v-r^*)-2r^*vG_t/G_1]}{4G_t+9K} - \frac{8(1-s^2)^{1/2}}{4G_t+9K}\left[\left(G_1+\frac{9Kr^*}{4}\right)\left(G_1+\frac{9Kv}{2}\right)+\frac{9K}{4}G_1s(2v-r^*)\right]^{1/2}; \tag{26}$$

Parabolic:

$$\frac{|\sigma_{zz}-\sigma_{rr}|}{2G_1} > 1; \tag{27}$$

Hyperbolic:

$$\frac{E}{G_l} < \frac{8(1-s^2)G_l + 9K[2v + r^* + s(2v - r^*) - 2r^* v G_t / G_l]}{4G_t + 9K} - \frac{8(1-s^2)^{1/2}}{4G_t + 9K}\left[\left(G_l + \frac{9Kr^*}{4}\right)\left(G_l + \frac{9Kv}{2}\right) + \frac{9K}{4} G_l s(2v - r^*)\right]^{1/2}. \quad (28)$$

The elliptic regime can be subdivided into portions where the roots of (25) are complex (EC) and where they are imaginary (EI). The elliptic imaginary subregime (EI) is given by (26) if the negative sign in front of the square root term becomes positive.

As shown from (3), the Rudnicki–Rice (1975) model suggests that the values of r^* and v depend on the sign of $(\sigma_{zz} - \sigma_{rr})/2G_l$. Consequently, the elliptic–parabolic (E/P) boundary is not symmetric with respect to $\sigma_{zz} = \sigma_{rr}$ and this differs from the plane strain analyses by Needleman (1979) and by Chau and Rudnicki (1990) (typical plots are given in Figs 8–10).

In general, if normality is not satisfied, shear band bifurcation may be possible in the pre-peak range of the axial stress–strain curve. To see this, let us assume E degrades more rapidly with deformation than other material parameters. In addition, for smooth yield surface, i.e. G_l is essentially the elastic shear modulus, shear band bifurcation becomes possible if E diminishes to the point where the hyperbolic region is entered near $s = 0$. Setting $s = 0$ in (28) and rearranging yields the critical value of E for shear band mode obtained by Rudnicki (1977):

$$E = \frac{\left\{G_l - \left[\left(G_l + \frac{9Kr^*}{4}\right)\left(G_l + \frac{9Kv}{2}\right)\right]^{1/2}\right\}^2}{G_t + 9K/4} - \frac{9Kr^* v}{2}. \quad (29)$$

As discussed by Rudnicki (1977), (29) actually corresponds to the critical value of E obtained by neglecting the difference between $\overset{\nabla}{\sigma}$ and $\dot{\sigma}$. A positive E is possible from (29) at strain localization although Rudnicki (1977) concluced that such a situation requires extreme values of material parameters. If normality is satisfied ($r^* = 2v$), it can be shown that (29) is always negative for positive G_t and K. As noted by Rudnicki and Rice (1975) for isotropic materials, if plastic normality is satisfied strain localization is not possible prior to peak applied stress in axisymmetric compression. The result here generalizes this conclusion to transversely anisotropic solids. More generally, Hill (1983) has shown, using the technique of splitting second-rank tensors at an interface into exterior and interior parts, that this conclusion, regarding the effect of normality on localization, is true for arbitrarily anisotropic solids.

The consequences of introducing transverse anisotropy can be illustrated by adopting the interpretation of G_l and G_t as reduced shear moduli and K as an elastic modulus, i.e. $G_l/K \approx 0$ and $G_t/K \approx 0$. With these simplifications, (29) further reduces to (Rudnicki, 1977)

$$E = G_l[2v + r^* - 2(2r^* v)^{1/2}] - 2G_l r^* v. \quad (30)$$

For shear band bifurcation to occur in the hardening range, it requires

$$\frac{G_t}{G_l} \leqslant \frac{(r^*/2v) + 1 - 2(r^*/2v)^{1/2}}{(r^*/2v)}. \quad (31)$$

The significance of normality and transverse anisotropy for possible pre-peak strain localization is illustrated in Fig. 1 by plotting G_t/G_l against $r^*/2v$. The cross-hatched region corresponds to shear band initiation at $E > 0$. As mentioned in Section 2, the Rudnicki–Rice (1975) model suggests that $r^*/2v > 1$ for compression and $r^*/2v < 1$ for tension. Therefore, if there is no transverse anisotropy ($G_t/G_l = 1$), pre-peak strain localization is excluded under compression because the isotropic line, $G_t/G_l = 1$, meets (31) only at $r^*/2v \to \infty$ for $r^*/2v > 1$. Introduction of transverse anisotropy in (1) enhances the possibility of the shear band mode in the hardening range ($E > 0$) under axisymmetric compression. For

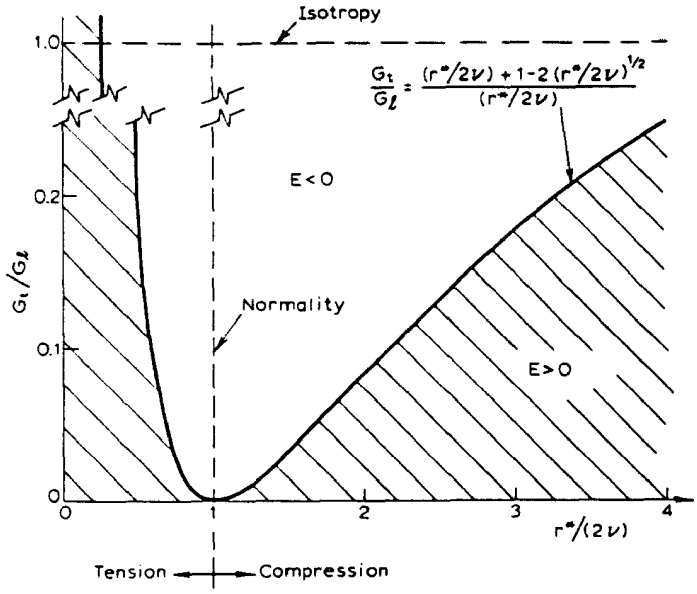

Fig. 1. Sketch depicts different portions in parameter space (G_t/G_l, $r^*/2\nu$) for which shear band bifurcation occurs at pre-peak ($E > 0$) or post-peak ($E < 0$) region. The cross-hatched areas are regions for which strain localization appears preceding the peak applied stress. The plot is based on eqn (31) which is for $K \gg G_l$ and $K \gg G_t$. The lines corresponding to normality ($r^* = 2\nu$) and isotropy ($G_t = G_l$) are also shown.

example, if $r^*/2\nu = 3$ [roughly corresponding to $\mu = 0.9$ and $\beta = 0.2$ in Rudnicki–Rice (1975) model], Fig. 1 suggests that shear band occurs at $E > 0$ for $G_t/G_l \leqslant 0.1786$. Such a value of G_t/G_l does, however, require a strong vertex effect. Conversely, for tension ($r^*/2\nu < 1$) pre-peak strain localization is possible even for $G_t = G_l$ if $r^*/2\nu < 1/4$. This value of $r^*/2\nu$ is possible, since (3) gives, for tension, r^* from 0 to 0.44 and 2ν from 0.44 to 0.70 for typical values of β (0.2–0.4) and μ (0.4–0.9) suggested by Rudnicki and Rice (1975). In addition, the occurrence of a minimum point at $r^*/2\nu = 1$ and $G_t/G_l = 0$ (as shown in Fig. 1) again demonstrates that pre-peak strain localization is not possible for transversely anisotropic solids satisfying normality.

Similar to the plane strain case (Needleman, 1979; Chau and Rudnicki, 1990), the ratio $\tan\theta = g_r/g_z$, in addition to satisfying (25), must not exceed $L/2a$ and the band must be vanishingly narrow to meet the traction-free condition on the sides at bifurcation. The angle θ at the transition from elliptic to hyperbolic regime satisfies

$$\tan\theta = \left[\frac{(1+s)(4E+18Kr^*\nu)}{(1-s)(4G_t+9K)}\right]^{1/4}, \tag{32}$$

where E can be evaluated by (28) with the $<$ sign replaced by an equal sign. Figure 2 shows θ versus $s(=(\sigma_{zz}-\sigma_{rr})/2G_l)$ for some combinations of material constants (assumed fixed with s) given in Table 1. The parameters r^* and ν used in Fig. 2 are evaluated assuming that μ and β are positive, as in Rudnicki and Rice's (1975) model, i.e. (3) is used. A typical range of μ and β suggested by Rudnicki and Rice (1975) is used in Table 1. Equation (3) gives a discontinuity of both r^* and ν across $s = 0$ and, hence, there is also a jump in bifurcation angle θ.

The predictions of (32) illustrated in Fig. 2 are consistent with experiments for various rocks. In particular, if s is negligible at localization, θ is found in the ranges 52°–57° for compression ($s < 0$) and 19°–36° for tension ($s > 0$) for the material parameters given in Table 1. Fracture angles observed experimentally by Brace (1964) and Mogi (1967) for various rocks (including dolomite, diabase, quartzite, granite and limestone) are in the ranges 58°–77° for compression and 0°–24° for extension. Therefore, the prediction based on (32) and (3) underestimates the bifurcation angle for compression but overestimates

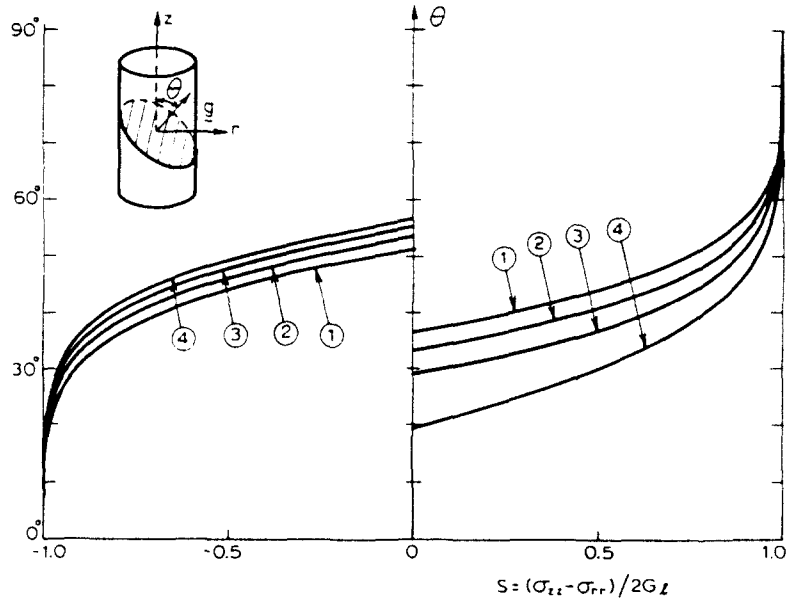

Fig. 2. The bifurcation angle θ, angle between normal to shear band and the axis of symmetry of the circular cylinder, on the elliptic–hyperbolic (E/H) boundary is shown against $(\sigma_{zz}-\sigma_{rr})/2G_1$. The parameters for each curve are given in Table 1.

Table 1. Various values of μ, β, G_t/G_1, K/G_1, r^* and 2ν used in plotting Fig. 2 (r^* and 2ν are evaluated based on eqn (3))

Curve	μ	β	G_t/G_1	K/G_1	$s<0$ r^*	$s<0$ 2ν	$s>0$ r^*	$s>0$ 2ν
1	0.4	0.2	1.0	100	1.90	1.39	0.44	0.69
2	0.4	0.4	0.75	100	1.90	1.90	0.44	0.44
3	0.6	0.4	0.5	5	2.59	1.90	0.23	0.44
4	0.9	0.2	0.5	5	4.25	1.39	−0.03	0.69

them for tension. Note, however, that a stronger non-normality (for example, curve 4 in Fig. 2) gives better agreement with experiments. To obtain higher values of θ for compression requires extreme values of material parameters [see Table I of Rudnicki (1977)].

The rough agreement of the prediction of (32) with experiments lends credence to the interpretation of r^* and ν based on comparison with Rudnicki and Rice's (1975) model. Therefore, this interpretation of r^* and ν (given by (3)) is used in the rest of this study except where otherwise stated.

The effects of non-normality and dilatancy on the bifurcation angle can be seen easily if E and G_t are negligible compared with K and $s = 0$ at the inception of strain localization. Then, as noted by Rudnicki (1977), eqn (32) can be approximated by $\tan\theta \approx (2r^*\nu)^{1/4}$. Therefore, only for incompressible solids satisfying normality, that is, for $2\nu = r^* = 1$, does $\theta = 45°$. Furthermore, the bifurcation angle θ increases with non-normality ($r^*/2\nu > 1$) and dilatancy in compression; in tension θ increases with dilatancy but decreases with non-normality ($r^*/2\nu < 1$).

5. DIFFUSE BIFURCATION MODES

Geometric diffuse bifurcation modes, appearing in elliptic, hyperbolic and parabolic regimes, are considered in this section. Special limits of diffuse modes, such as long wavelength necking and bulging modes and short wavelength surface rumpling modes, are emphasized.

Following Miles and Nuwayhid (1985), the diffuse bifurcation modes are assumed in the form

$$\chi(r,z) = X(r)\cos(\eta z), \tag{33}$$

where $\eta = k\pi/L, k = 1,2,\ldots$ and, hence, the end boundary condition (14) is satisfied identically on $z = 0$ and L. With the eigenmodes (33), the following governing equation of $X(r)$ is obtained

$$(AL_1^2 - \eta^2 BL_1 + \eta^4 C)X(r) = 0, \tag{34}$$

where the operator L_1 has been defined following (18) and A, B and C have been given in (22). Furthermore, since the lateral surface $r = a$ of the cylinder sustains no shear traction, substitution of (17)–(19) and (33) into (15) yields

$$(Y_2 - Y_4)\frac{1}{r}\frac{dX}{dr} + Y_2\frac{d^2X}{dr^2} + \eta^2\left[Y_3\left(\frac{1}{r^2}\int rX(r)\,dr\right) - Y_1X\right] = 0,$$

$$Y_6\frac{dX}{dr} - \eta^2 Y_5\left(\frac{1}{r}\int rX(r)\,dr\right) = 0, \tag{35}$$

on $r = a$. And we have used the following definitions for $Y_i, i = 1,2,\ldots,6$,

$$\begin{aligned} Y_1 &= 1 - r^*\sigma_{rr}/(2\nu\sigma_m), & Y_2 &= \sigma_{rr}(4G_t + 9K)/(18K\nu\sigma_m), \\ Y_3 &= (2G_t - \sigma_{rr})(9Kr^*\nu + 2E)/(9K\nu\sigma_m), & Y_4 &= -(2G_t - \sigma_{rr})/\sigma_m, \\ Y_5 &= \sigma_{zz}(9Kr^*\nu + 2E)/(9K\nu\sigma_m), & Y_6 &= 1 - \sigma_{zz}/\sigma_m. \end{aligned} \tag{36}$$

The "follower type" confining stress (Cheng *et al.*, 1971; Vardoulakis, 1983) can be obtained by simply setting $\sigma_{rr} = 0$ in (36).

The general solutions of (34) are of the form

$$X(r) = A_1 J_0(\eta\rho_1 r) + A_2 J_0(\eta\rho_2 r), \tag{37}$$

where J_0 is the Bessel function of the first kind of order zero. Substitution of (37) into (34) reveals, as expected, that the ρ_m, $m = 1,2$ satisfy (25), the equation for evaluating the direction of the shear band (g_r/g_z); hence, the regime classification given in Section 4 equally applies here. Alternatively, (34) can be factored as

$$(L_1 + \eta^2\rho_1^2)(L_1 + \eta^2\rho_2^2)X(r) = 0. \tag{38}$$

Since the evaluation of the eigenvalue equation is similar to that for plane strain (Hill and Hutchinson, 1975) and to that for axisymmetric deformation (Cheng *et al.*, 1971; Vardoulakis, 1983; Miles and Nuwayhid, 1985), the results are only summarized briefly in the following subsections.

5.1. *The elliptic regime*

As mentioned earlier, the elliptic regime can be subdivided into portions where the roots are complex (EC) and imaginary (EI). In EC, the roots for (25) are $\rho = p + iq$ and its conjugate $\bar{\rho} = p - iq$. The solution form is

$$X(r) = \mathrm{Re}[AJ_0(\eta\rho r)], \tag{39}$$

where Re[...] denotes the real part of [...]. The quantities p and q are defined as

$$p^2-q^2 = -B/2A, \quad p^2+q^2 = (C/A)^{1/2}, \tag{40}$$

where A, B and C are given by (22).

The corresponding eigenvalue equation from (35) is

$$\mathrm{Im}\{J_1(\gamma\bar{\rho})(Y_5+\bar{\rho}^2Y_6)[J_1(\gamma\rho)(Y_3+\rho^2Y_4)-\gamma\rho J_0(\gamma\rho)(Y_1+\rho^2Y_2)]\} = 0, \tag{41}$$

where Im[...] means the imaginary part of [...] and $\gamma = \eta a$ (or $\gamma = k\pi a/L$).

For the EI subregime, the pure imaginary roots of (25) are $\rho_1 = ip$ and $\rho_2 = iq$ where p and q are real positive and are related to the material parameters as

$$p^2-q^2 = (B^2-4AC)^{1/2}/A, \quad p^2+q^2 = B/A, \tag{42}$$

and again A, B and C are given by (22). The solution for $X(r)$ becomes

$$X(r) = A_1I_0(\eta pr)+A_2I_0(\eta qr), \tag{43}$$

where I_0 is the modified Bessel function of order zero.

The boundary condition on $r = a$ (35) yields the eigenvalue equation

$$\frac{[Y_5-Y_6p^2]I_1(\gamma p)}{[Y_5-Y_6q^2]I_1(\gamma q)} = \frac{[Y_3-Y_4p^2]I_1(\gamma p)-\gamma p[Y_1-Y_2p^2]I_0(\gamma p)}{[Y_3-Y_4q^2]I_1(\gamma q)-\gamma q[Y_1-Y_2q^2]I_0(\gamma q)}, \tag{44}$$

for the EI subregime.

Both long wavelength limit, $\gamma \to 0$, and short wavelength limit, $\gamma \to \infty$, of the eigenvalue equations in EC and EI are considered here. For small values of γ, J_n can be written in series representation (Abramowitz and Stegun, 1964) then substituted into (41) to yield the long wavelength limit for EC:

$$\sigma_{zz} = \frac{E}{2\nu}\left[\frac{1+\sigma_{rr}[2/9K-r^*(1-\nu)/E]}{1+2\sigma_{rr}/9K\nu}\right]+0(\gamma^2). \tag{45}$$

The first term on right side is the maximum load point given by (13). Therefore, the long wavelength necking or bulging mode occurs at the maximum load point independently of whether the constitutive relation satisfies normality. This observation is consistent with the result obtained by Miles and Nuwayhid (1985) for long wavelength necking mode under uniaxial tension. The maximum load point, eqn (45), is sketched as curve A in Figs 8–10.

To consider the long wavelength limit in EI, the series representation of the modified Bessel function is substituted into (44) to yield (45) again. Therefore, the long wavelength bifurcation mode (45) continues across the EI/EC boundary.

For the short wavelength limit, $\gamma \to \infty$, substitution of the asymptotic forms of J_n and I_n with large arguments (Abramowitz and Stegun, 1964) leads to the requirement

$$(Y_1Y_6-Y_2Y_5)(AC)^{1/2}+AY_1Y_5+Y_2(CY_6-BY_5) = 0, \tag{46}$$

for the EC subregime. If $\sigma_{rr} = 0$, $K \to \infty$ and $r^* = 2\nu = 1$, this short wavelength limit can be simplified to

$$\frac{\sigma_{zz}}{(E+G_1)} = 1+\frac{\sigma_{zz}}{(E+G_1)}\left[\frac{2G_1-\sigma_{zz}}{2G_1+\sigma_{zz}}\right]^{1/2}. \tag{47}$$

The eigenvalue equation (47) has been obtained for an incompressible half-space satisfying normality by Biot (1965) and Bassani *et al.* (1980). Hill and Hutchinson (1975) and Young (1976) also obtained the same bifurcation condition for short wavelength diffuse mode

under plane strain conditions. Similarly, appropriate specializations of the short wavelength diffuse mode by Needleman (1979) and Chau and Rudnicki (1990) also lead to (47). The solution to (46) is shown as curve B in Figs 8–10. Furthermore, the short wavelength limit never intersects with the E/P boundary because there is no root to (46) on either compressive or tensile E/P boundaries ($s = -1$ and $s = 1$, respectively).

Substitution of the asymptotic form of the modified Bessel function with large argument into (44) again leads to (46) for the EI subregime; hence, the short wavelength surface rumpling modes continue across the EI/EC boundary.

In the plane strain bifurcation analysis, some diffuse bifurcation modes can be excluded from portions of the elliptic regime (Needleman, 1979; Chau and Rudnicki, 1990). However, due to mathematical complexity, such considerations are not straightforward in the present axisymmetric case.

5.2. *The parabolic regime*

In parabolic regime, the roots for (25) are p and iq. The general solutions are in the form

$$X(r) = A_1 J_0(\eta p r) + A_2 I_0(\eta q r). \tag{48}$$

The real constants, p and q, are defined as

$$p^2 + q^2 = (B^2 - 4AC)^{1/2}/|A|, \quad p^2 - q^2 = -B/A. \tag{49}$$

Substitution of (48) into (35) leads to the following eigenvalue equation for parabolic regime:

$$\frac{[Y_5 + Y_6 p^2] J_1(\gamma p)}{[Y_5 - Y_6 q^2] I_1(\gamma q)} = \frac{[Y_3 + Y_4 p^2] J_1(\gamma p) - \gamma p J_0(\gamma p)[Y_1 + Y_2 p^2]}{[Y_3 - Y_4 q^2] I_1(\gamma q) - \gamma q I_0(\gamma q)[Y_1 - Y_2 q^2]}. \tag{50}$$

Bifurcation of diffuse modes becomes possible as soon as the parabolic regime is entered. To see this, we can first consider the short wavelength limit of (50). This limit requires that $\tan(\gamma p)$ equals a quotient with both the numerator and the denominator being a polynomial of p and q having coefficients involving only Y_1, Y_2, Y_5 and Y_6. This relation is found similar to that for the parabolic eigenvalue equation for a rectangular specimen under plane strain deformations. Consequently, the arguments employed by Hill and Hutchinson (1975) and by Needleman (1979) for the eigenvalue equation on the tensile elliptic-parabolic boundary in plane strain case (note $\gamma p \to \infty$ for fixed value of γ in their case) can also be applied here. Moreover, as already mentioned, we are considering the short wavelength limit ($\gamma \to \infty$). Therefore, the same argument equally applies for the compressive elliptic-parabolic boundary where p is bounded. More specifically, as s approaches 1 from above (or s approaches -1 from below), $\tan(\gamma p)$ oscillates between $\pm\infty$ in an infinite sequence of intervals bounded below by $s = 1$ (or bounded above by $s = -1$). This implies, as noted by Hill and Hutchinson (1975), that in any finite interval closed from below by $s = 1$ (or from above by $s = -1$) there is an infinite sequence of eigenvalues for the short wavelength limit of (50). In particular, there is an infinite sequence of eigenvalues available in the vicinities of both the tensile and compressive E/P boundaries for some sufficiently large k (note that $\gamma = k\pi a/L$). Therefore, short wavelength diffuse modes and shear band modes are always available simultaneously once the parabolic regime is entered.

5.3. *The hyperbolic regime*

In the hyperbolic regime, the solution modes are in the form

$$X(r) = A_1 J_0(\eta p r) + A_2 J_0(\eta q r). \tag{51}$$

The real roots for (25) are p and q and they satisfy

$$p^2+q^2=-B/A,\quad p^2-q^2=(B^2-4AC)^{1/2}/A. \tag{52}$$

The eigenvalue equation is

$$\frac{[Y_5+Y_6p^2]J_1(\gamma p)}{[Y_5+Y_6q^2]J_1(\gamma q)}=\frac{[Y_3+Y_4p^2]J_1(\gamma p)-\gamma p[Y_1+Y_2p^2]J_0(\gamma p)}{[Y_3+Y_4q^2]J_1(\gamma q)-\gamma q[Y_1+Y_2q^2]J_0(\gamma q)}. \tag{53}$$

Expanding (53) in ascending powers of γ gives (45) again. Hence, the long wavelength necking and bulging modes continue through the elliptic–hyperbolic boundary. The short wavelength limit ($\gamma\to\infty$) of (53) requires that $\tan(\gamma p)$ is equal to a quotient with $f_1(p,q)+\tan(\gamma q)f_2(p,q)$ as numerator and $f_2(p,q)+\tan(\gamma q)f_1(p,q)$ as denominator. f_1 and f_2 are polynomials of p and q with coefficients involving only Y_1, Y_2, Y_5 and Y_6. This relation for the short wavelength limit is again found to be similar to the form of the hyperbolic eigenvalue equation under plane strain condition (Chau and Rudnicki, 1990; Needleman, 1979). Consequently, the same arguments discussed by Needleman (1979) show that bifurcation into some sufficiently short wavelength mode is possible as soon as the hyperbolic regime is entered.

By comparing this section to Needleman (1979) and Chau and Rudnicki (1990), we find a close resemblance between diffuse mode analyses for axisymmetric and plane strain states. More specifically, although the eigenmodes for plane strain and axisymmetric deformation are different, the results obtained by the diffuse mode analyses share some common characteristics. In particular, for both cases the long wavelength limit coincides with the maximum load point; the surface rumpling modes in the elliptic regime are of the same form.

Although geometric diffuse modes in both hyperbolic and parabolic regimes are found to be mathematically admissible, they are of less interest. As soon as the hyperbolic or parabolic regime is entered, the shear band mode is expected to dominate. However, elliptic diffuse modes may play a significant role in the development of subsequent localization and will be investigated numerically next.

6. NUMERICAL RESULTS FOR ELLIPTIC DIFFUSE MODE

In this section, a standard numerical search procedure [e.g. Section 9.3 of Press *et al.* (1989)] was used to evaluate the bifurcation stresses to six significant digits at various values of γ ($=k\pi a/L$) in the EC subregime. First, the EC subregime was identified using (26). Then, (41) is used to search for the root of $(\sigma_{zz}-\sigma_{rr})/2G_1$ at each fixed γ. If no eigenvalue was found within the EC subregime, the search is discontinued.

The material parameters in (1), in general, change in a possibly complex way with stress. However, in order to gain insight into their effect on the occurrence of diffuse bifurcations, solutions to (41) in Fig. 3 are given by holding all parameters, except one, constant.

6.1. *Diffuse mode with finite* γ

In Fig. 3(a), typical eigenvalue surfaces for a solid not satisfying normality ($\mu\neq\beta$) at various values of E/G_1 are obtained for both tension and compression. The long wavelength limit ($\gamma=0$), eqn (45) (corresponding to curve A in Fig. 8), coincides with the y-axis in Fig. 3(a). Under compression, for increasing $|\sigma_{zz}/2G_1|$, the first eigenvalue surface we intersect is the one for $E/G_1=0$. More specifically, the lowest possible bifurcation stress is always at peak ($E/G_1=0$). However, the actual value of E/G_1 may not be zero when $|\sigma_{zz}/2G_1|$ intersects the eigensurface of $E/G_1=0$; hence (41) may not be satisfied at that point. In particular, the actual bifurcation may occur pre-peak ($E>0$) if $|\sigma_{zz}/2G_1|$ increases more rapidly than the drop of E/G_1 such that (41) is satisfied for some positive E/G_1. Note that the eigenvalue surfaces in compression ($\sigma_{zz}/2G_1<0$) always have a maximum point (or smallest compressive stress level), which occurs at γ somewhere between two and three, for a fixed E/G_1 as shown in Fig. 3(a).

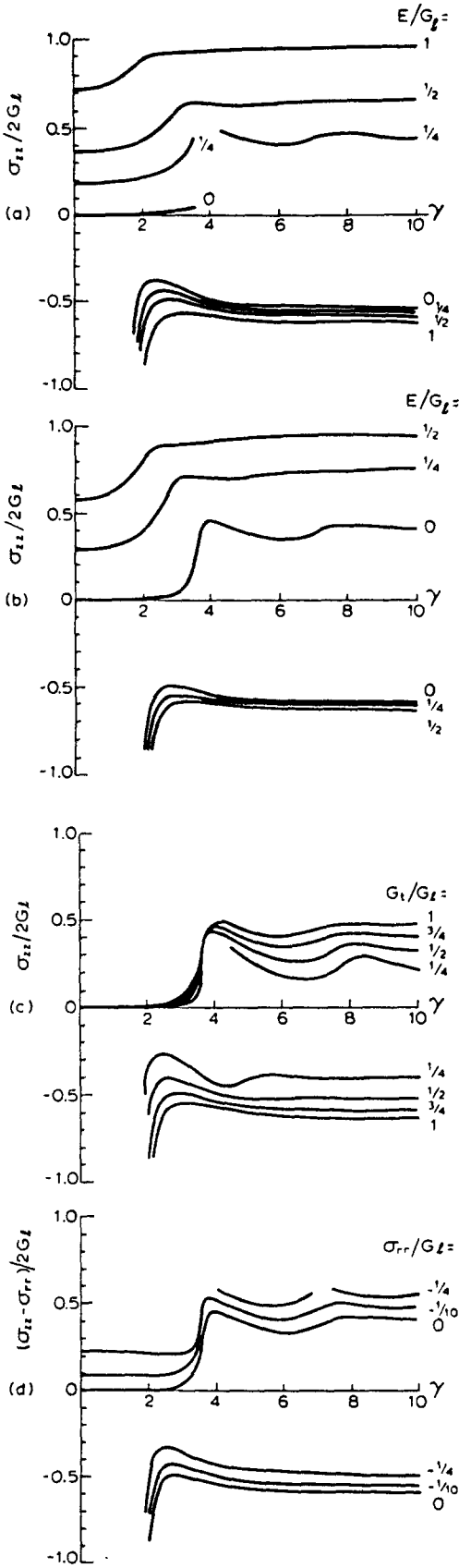

Fig. 3. Bifurcation stresses for EC diffuse modes with finite γ ($=k\pi a/L$): (a) changing E/G_l with $\mu = 0.6$, $\beta = 0.2$, $G_t/G_l = 0.75$, $G_l/K = 0.2$, and $\sigma_{rr}/G_l = 0$; (b) changing E/G_l with $\mu = \beta = 0.4$, $G_t/G_l = 0.75$, $G_l/K = 0.2$, and $\sigma_{rr}/G_l = 0$; (c) changing G_t/G_l with $\mu = \beta = 0.4$, $E/G_l = 0$, $G_l/K = 0.2$, and $\sigma_{rr}/G_l = 0$; and (d) changing σ_{rr}/G_l with $\mu = \beta = 0.4$, $E/G_l = 0$, $G_l/K = 0.2$, and $G_t/G_l = 0.75$.

Similar eigenvalue surfaces are plotted in $(\sigma_{zz}/2G_1, \gamma)$-space in Fig. 3(b) for a solid satisfying normality ($\mu = \beta$). To satisfy the eigenvalue equation a higher stress level ($|\sigma_{zz}|/2G_1$), in both tension and compression, is required for the same E/G_1 compared with Fig. 3(a). Thus, deviations from normality promote diffuse bifurcations in EC.

The effect of transverse anisotropy on EC diffuse modes occurring at peak ($E/G_1 = 0$) is illustrated in Fig. 3(c) by plotting the eigenvalue surfaces for various values of G_t/G_1. The drop of G_t/G_1 from unity reduces the eigenstress significantly at peak ($E/G_1 = 0$). That is, the introduction of transverse anisotropy promotes diffuse modes in both tension and compression. Again, the maximum eigenstress in compression occurs at γ between two and three.

Since the most common testing configuration for geological materials involves a constant confining stress, the effects of lateral stress are examined in Fig. 3(d). As the compressive confining stress increases, the eigenstress ($|\sigma_{zz} - \sigma_{rr}|/2G_1$) increases in tension but decreases in compression. More specifically, compressive confining stress promotes diffuse bifurcation modes in compression but retards them in tension.

Numerical calculations reveal that the effects on the eigenstress of decreasing G_t/K below 1/5 are insignificant for finite γ (< 10). Furthermore, the eigenvalue surface is suppressed by G_t/K greater than one.

As shown in Fig. 3(a–d), the smallest eigenstress level always appears at γ between two and three under compression. Typical radius to length ratios (a/L) of rock specimens used in experiments are between 1/4 [e.g. Wawersik and Fairhurst (1970) and Hadley (1975)] and 1/6 [e.g. Mogi (1967) and Scholz (1968)]. The eigenmodes, which give γ ($= k\pi a/L$) between two and three, are those with wave number $k = 3$ and $k = 4$ or 5 for $a/L = 1/4$ and $a/L = 1/6$, respectively. Combining the definition of v_r in terms of $\chi(r, z)$ and the eigenmode (33) reveals that v_r is proportional to $\cos(k\pi z/L)$. Such eigenmodes appear to be the earliest diffuse modes available under compression and are sketched in Fig. 4(a) for $k = 3$ and $a/L = 1/4$ and in Fig. 4(b) for $k = 4$ and $a/L = 1/6$. Note that the bulging mode ($k = 1$) is not possible for these specimen sizes according to Fig. 3(a–d). Further implications of these diffuse modes in compression on strain localizations are discussed in Section 7.

Under tension, as shown in Fig. 3, the minimum eigenstress is always at $\gamma = 0$, i.e. the maximum load point, for any fixed value of E/G_1. These numerical results suggest that, similar to the plane strain case (Chau and Rudnicki, 1990), the long wavelength diffuse mode is always the first bifurcation encountered in the EC subregime under tension. As shown in Fig. 3, the eigenstress for diffuse modes appearing at peak ($E = 0$) increases slowly for γ less than about three under tension. Then, for solids satisfying normality, as shown in Fig. 3(b–d), the eigenstress rises more rapidly for γ between three and four before forming

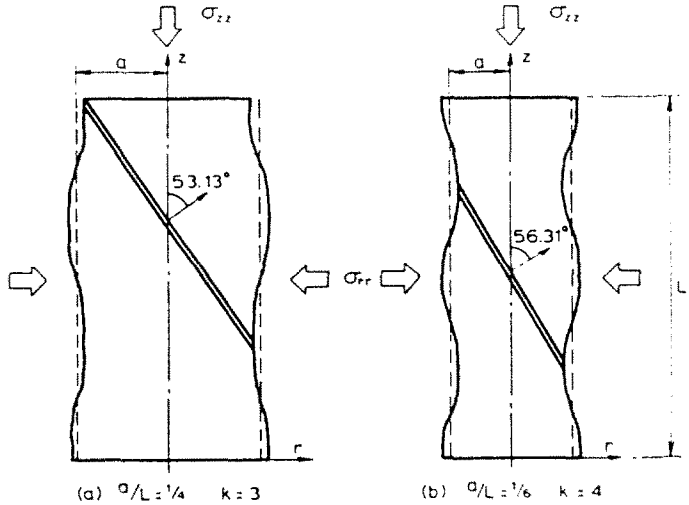

Fig. 4. Sketches illustrate the earliest possible pre-peak diffuse mode under compression. Possible shear band localization triggered by diffuse mode is also shown. The sketches are for: (a) $a/L = 1/4$ and $k = 3$; and (b) $a/L = 1/6$ and $k = 4$.

a hump-shaped curve; for solids that do not obey normality, as shown in Fig. 3(a), diffuse modes with γ greater than 3.5 are not possible at peak applied stress ($E = 0$). Since v_r is proportional to $\cos(k\pi z/L)$, for a specimen of finite size (non-zero a/L), $k = 2$ corresponds to the necking mode. For the material parameters used in Fig. 3, it can be shown that, as long as $a/L < 7/4\pi$, necking is possible at peak applied stress ($E = 0$) under tension. Necking may actually appear pre-peak (see, for example, (45) or curve A in Figs 8–10) depending on the evolution of material parameters under loadings.

6.2. *The short wavelength diffuse mode* ($\gamma \to \infty$)

Eigenvalue surfaces given in Fig. 3(a–d) are restricted to the finite wave number k ($\gamma < 10$). For large γ, or the short wavelength limit, (46) is solved numerically for various values of compressive confining stress and plotted in Fig. 5. The cross-hatched regime corresponds to the portion in the parameter space where the surface rumpling mode is possible preceding the peak applied stress ($E = 0$). The short wavelength limit of the diffuse mode may appear pre-peak if $|\sigma_{zz} - \sigma_{rr}|/2G_l$ increases more rapidly than the drop of E/G_l. As depicted in Fig. 5(a, b), there are two separate cross-hatched regions, one on the compressive side and one on the tensile side, in the parameter space. However, as shown in Fig. 5(c, d), as the compressive confining stress level increases the two separate regions connect. Consequently, surface undulation becomes possible even under hydrostatic stress, i.e. $\sigma_{zz} = \sigma_{rr}$. Therefore, compressive confining stress is conducive to the appearance of short wavelength diffuse mode. Note that, in Fig. 5, we have assumed that r^* and v are independent of the sign of s, that is, the interpretation of Fig. 5 is not restricted to the Rudnicki–Rice (1975) model. Such interpretations of r^* and v apply also to Figs 6 and 7.

For uniaxial tension and compression ($\sigma_{rr} = 0$), the condition for short wavelength mode at peak applied stress ($E = 0$) can be obtained from (46) as

$$\frac{\sigma_{zz}}{r^* G_l} = 1 + \frac{\sigma_{zz}}{r^* G_l}\left\{\left(\frac{r^*}{2v}\right)\left(\frac{4G_l}{9K} + 1\right)\left[\frac{2G_l - \sigma_{zz}}{2G_l + \sigma_{zz}}\right]\right\}^{1/2}. \tag{54}$$

The effect of transverse anisotropy on the short wavelength diffuse mode is investigated by plotting $r^*/2v$ against $\sigma_{zz}/2G_l$ in Fig. 6 for zero G_t/K. Again, the cross-hatched regions

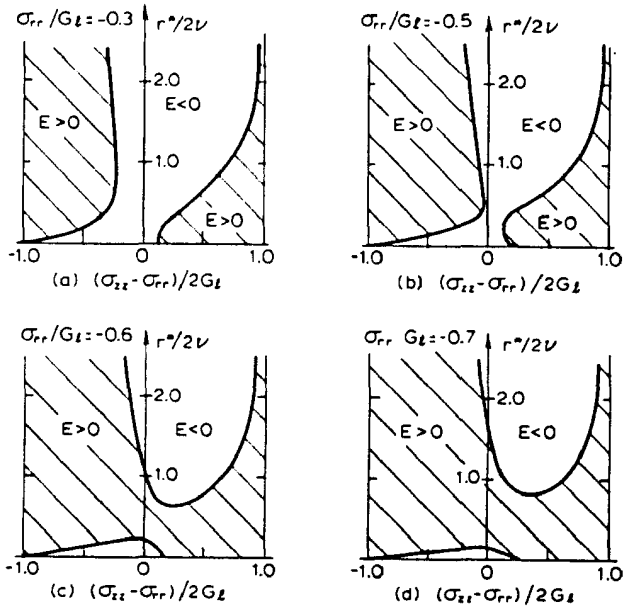

Fig. 5. Sketches depict different portions in $(r^*/2v, \sigma_{zz}/2G_l)$-space for which short wavelength diffuse modes may occur at pre-peak ($E > 0$). The cross-hatched areas are regions for which surface rumpling may appear preceding the peak applied stress. Material parameters used are $v = 1$, $G_t/G_l = 1/4$, $G_l/K = 1/4$, and with (a) $\sigma_{rr}/G_l = -0.3$; (b) $\sigma_{rr}/G_l = -0.5$; (c) $\sigma_{rr}/G_l = -0.6$; and (d) $\sigma_{rr}/G_l = -0.7$.

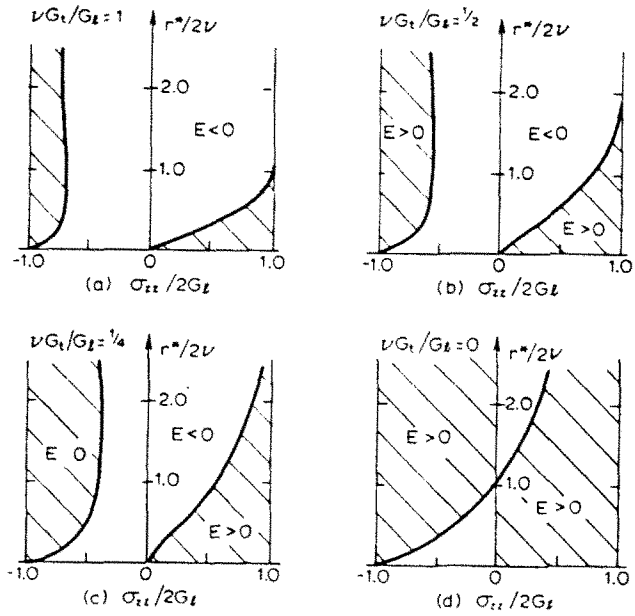

Fig. 6. Same as Fig. 5 for $G_t/K = 0$ and with (a) $\nu G_t/G_l = 1$; (b) $\nu G_t/G_l = 1/2$; (c) $\nu G_t/G_l = 1/4$; and (d) $\nu G_t/G_l = 0$.

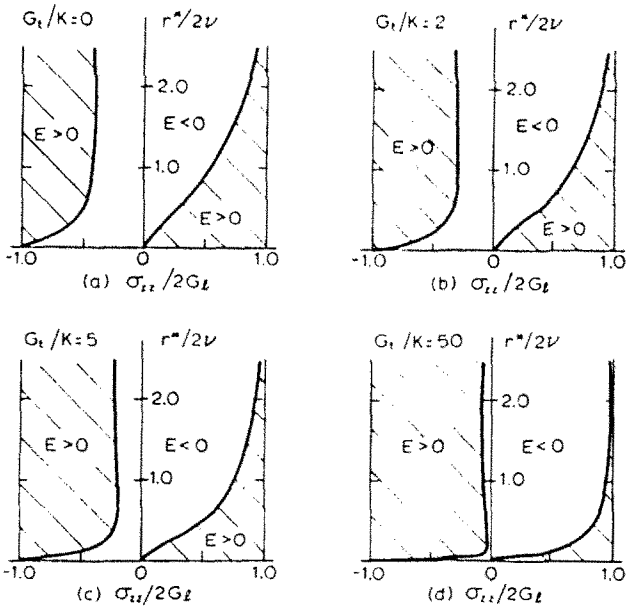

Fig. 7. Same as Fig. 5 for $\nu G_t/G_l = 1/4$ and with (a) $G_t/K = 0$; (b) $G_t/K = 2$; (c) $G_t/K = 5$; and (d) $G_t/K = 50$.

correspond to the parameter space where surface rumpling mode can appear pre-peak ($E > 0$). As $\nu G_t/G_l$ decreases both compressive and tensile cross-hatched regions expand correspondingly. That is, a stronger transverse anisotropy, corresponding to a smaller $\nu G_t/G_l$, reduces the eigenstress level ($|\sigma_{zz}|/2G_l$) required for pre-peak surface wrinkle mode. The two separate cross-hatched regions finally meet at $r^*/2\nu = 1$ as $\nu G_t/G_l$ approaches zero. Thus, the surface rumpling mode becomes possible at peak even for small $\sigma_{zz}/2G_l$ if $\nu G_t/G_l$ is negligible. Again, surface modes may appear at some positive E/G_l if $|\sigma_{zz}|/2G_l$ increases faster than the drop of E/G_l. More specifically, the introduction of transverse anisotropy enhances the appearance of the short wavelength diffuse mode. This conclusion is the same as those for diffuse modes with finite γ (see Fig. 3(c)).

Alternatively, (54) can be plotted for varying G_t/K but fixed $\nu G_t/G_1$ as shown in Fig. 7. As shown in Fig. 7(a–d), when the in-plane bulk modulus K decreases the cross-hatched portions expand in the compressive regime but shrink in the tensile one. In short, in-plane compressibility promotes the appearance of pre-peak surface undulation under compression but retards them under tension.

As mentioned previously, the values of r^* and ν used for Figs 5–7 are independent of Rudnicki–Rice (1975) model; that is, (3) is not used. However, as mentioned in Section 2, the Rudnicki–Rice (1975) model suggests that $r^*/2\nu > 1$ for compression. As shown in Figs 5–7, (54) changes slowly with the increase of $r^*/2\nu$ for $r^*/2\nu > 1$. That is, the short wavelength diffuse mode is relatively less sensitive to non-normality compared with the diffuse mode for finite γ.

7. DISCUSSION

The incremental constitutive parameters in (1) are, in general, functions of deformation and stress state. For example, for brittle rocks, ν increases rapidly with deformation after the onset of dilatancy but decreases with confining pressure [e.g. Brace *et al.* (1966)]. Thus, the interpretations of the present analysis can be extremely complicated and difficult. However, if r^*, ν, G_1, G_t and K vary much more slowly with deformation than the tangent modulus E, the situation is simplified considerably. And we further assume that the confining stress is constant during the whole course of deformation.

With the above simplifications, Fig. 8 shows a typical case of the response regimes when $\sigma_{rr} = 0$. Since both r^* and ν, according to (3), change values across $\sigma_{zz} = 0$, the response regimes are not symmetric with respect to $\sigma_{zz} = 0$, and hence, differ from the plane strain analysis (see Figs 3–5 of Chau and Rudnicki, 1990).

In general, the maximum load point (13) and the elliptic–hyperbolic (E/H) boundary do not intersect $s = 1$ at the same point. For example, if

$$E(4G_t + 9K) > 9K\nu(2 - r^*G_t/G_1)(\sigma_{zz}^{\max} - \sigma_{rr}), \tag{55}$$

the maximum load point cuts $s = 1$ on the EI/P boundary or otherwise the maximum load point meets $s = 1$ on the H/P boundary.

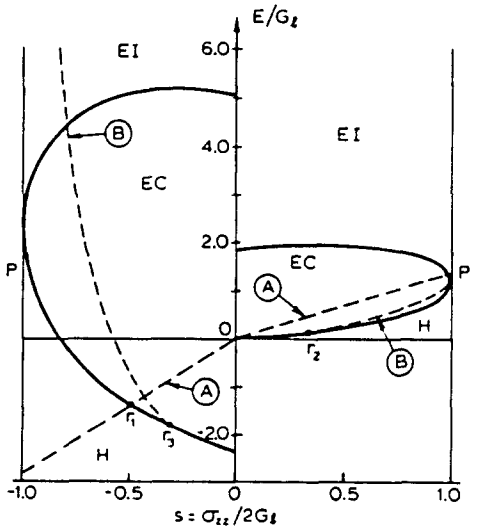

Fig. 8. Sketch shows different regimes of bifurcation, including hyperbolic (H), elliptic complex (EC), elliptic imaginary (EI) and parabolic (P), in the parameter space $(E/G_1, (\sigma_{zz} - \sigma_{rr})/2G_1)$ for $\sigma_{rr} = 0$. The material parameters r^* and ν are evaluated using eqn (3) and assuming μ and β are positive in Rudnicki and Rice's (1975) model. Long wavelength limit (curve A) and short wavelength limit (curve B) are also shown. Sketch is for $G_t = 0.75\,G_1$, $K = 5\,G_1$, $\mu = 0.6$, and $\beta = 0.2$.

According to Fig. 8, for tension ($\sigma_{zz} > 0$), strain localization seems always possible in the hardening range ($E > 0$) for the constitutive parameters considered ($G_t = 0.75G_1$, $K = 5G_1$, $\mu = 0.6$ and $\beta = 0.2$). If E/G_1 drops rapidly and the loss of ellipticity occurs between $\sigma_{zz} = 0$ and r_2, the long wavelength necking mode (surve A) may precede the shear band mode depending on the actual slenderness ratio of the specimen. However, the numerical solution of (41) (see Fig. 3) suggests that a necking mode, but not necessarily the long wavelength mode, is always possible in the EC subregime even for finite specimen size ($a/L \neq 0$ but less than $7/4\pi$). For slowly decreasing E/G_1, if a sufficiently large value of $\sigma_{zz}/2G_1$ can be sustained, the short wavelength surface rumpling (curve B) precedes loss of ellipticity but occurs after the maximum load (curve A). If G_1 is interpreted as a vertex reduced shear modulus such that loss of ellipticity occurs on the EI/P boundary between

$$4\nu > E/G_1 > \frac{18K\nu(2-r^*G_t/G_1)}{4G_t+9K}. \tag{56}$$

then the necking mode always precedes the shear band mode available on the E/P boundary (note that (55) is satisfied for the constitutive parameters used in Fig. 8). However, if the parabolic regime is entered at $E/G_1 > 4\nu$, no necking mode precedes the initiation of the shear band. In compression ($\sigma_{zz} < 0$), pre-peak shear band, or strain localization, is possible only if loss of ellipticity occurs at sufficiently large values of $\sigma_{zz}/2G_1$, i.e. yield surface vertex effect dominates in the interpretation of G_1. In such circumstances, surface rumpling always precedes the localization. If G_1 is essentially the elastic modulus during the whole deformation path, localization occurs relatively late in the post-peak applied stress regime ($E < 0$) near $s = 0$. This is consistent with the conclusions by Rudnicki and Rice (1975) and by Rudnicki (1977). In such situations, both long wavelength bulging and short wavelength surface bifurcations may precede shear band bifurcation. In particular, if the exit to hyperbolic regime occurs between $\sigma_{zz} = 0$ and r_3, bulging mode is always possible before the onset of localization depending on the actual specimen dimensions. If loss of ellipticity happens between r_1 and r_3, short wavelength surface mode precedes shear band mode but occurs after the long wavelength bulging mode. Further, the short wavelength diffuse mode is always available prior to the entry to the hyperbolic regime between r_1 and $E/G_1 = 0$.

However, as shown in Fig. 3, some intermediate diffuse modes, between long and short wavelength limits, with finite wave number are actually possible preceding or at peak applied stress. That is, the pre-peak diffuse bifurcation mode, as depicted in Fig. 4, is always possible before the transition from the EC subregime to the hyperbolic regime. Then, once (41) is satisfied for some positive E/G_1 during the evolution of deformation, diffuse modes such as those shown in Fig. 4 occur preceding peak applied stress. Because these diffuse modes appear in the elliptic regime before localization, they may affect the subsequent development of localization. Roughly speaking, these deformed states may be viewed as initial geometric imperfection of the specimen. By using finite element method, Tvergaard *et al.* (1981) found that geometric imperfection plays an important role in governing the subsequent shear band pattern of a rectangular specimen under plane strain tension. However, a similar numerical simulation is not available for cylindrical specimens under compression. Nevertheless, such pre-peak or at peak diffuse bifurcation modes may precipitate localization of deformations. In particular, as shown in Fig. 4, the angle between the z-axis and the normal of the line joining two opposite adjacent troughs are 53.13° and 56.31° (by assuming a small amplitude of diffuse modes) for $a/L = 1/4$ and $a/L = 1/6$ respectively. These angles are just about the angle of faulting predicted by (32) for small $(\sigma_{zz}-\sigma_{rr})/2G_1$ under compression (e.g. see Fig. 2). This coincidence leads naturally to the suspicion that such diffuse modes trigger the pre-peak localization of deformation observed for rocks. Of course, the geometric modes depicted in Fig. 4 may not appear at all depending on the evolution of material parameters with deformation and whether the eigenvalue equation (41) is satisfied. Although the hypothesis seems plausible, numerical calculations, similar to those of Tvergaard *et al.* (1981), are required to further investigate and clarify such a possibility.

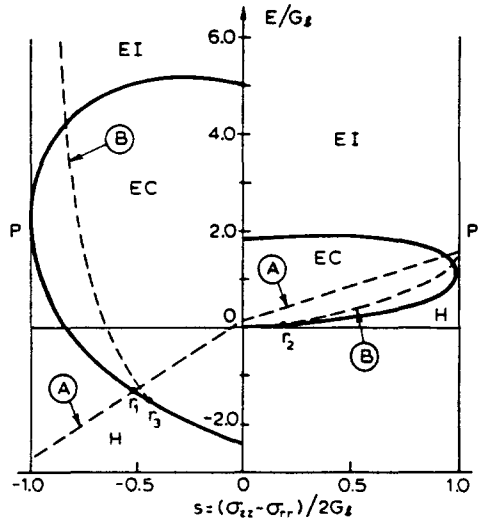

Fig. 9. Same as Fig. 8 for tensile lateral stress of $\sigma_{rr} = 0.2\,G_1$.

Consequently, a localized shear band may appear much earlier than the theoretical prediction, which is based on the loss of ellipticity, given in Section 4. Therefore, the hypothesis that a pre-peak diffuse mode triggers localization of deformation provides a possible explanation for those experimental observations summarized by Santarelli and Brown (1989).

For tensile lateral stress ($\sigma_{rr} = 0.2G_1$), as shown in Fig. 9, the long wavelength limit (curve A) shifts upward and cuts $s = 0$ at

$$\frac{E}{G_1} = \frac{\sigma_{rr}[r^*(1-\nu)+2\nu(1+2\sigma_{rr}/9K\nu)]}{G_1(1+2\sigma_{rr}/9K)}, \tag{57}$$

and the short wavelength limit (curve B) pierces the EC/EI boundary to continue in EI subregime. That is, tensile lateral stress favors the appearance of both short wavelength surface mode and long wavelength necking mode for $s > 0$. Furthermore, the compressive E/H boundary between r_1 and r_3 shrinks considerably as curve B moves upwards faster than curve A. However, the overall response is similar to that described for Fig. 8.

Figure 10 shows a situation for compressive lateral stress of $\sigma_{rr} = -0.2G_1$. In this case, both curves A and B move towards the E/H boundary. More specifically, the shear band

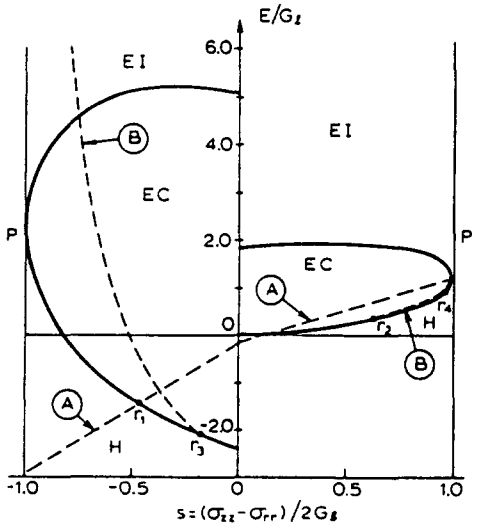

Fig. 10. Same as Fig. 8 for compressive lateral stress of $\sigma_{rr} = -0.2\,G_1$.

mode, appearing in the hardening regime, precedes the long wavelength necking mode when the exit to the hyperbolic regime occurs near $s = 0$. The short wavelength mode (curve B) is eliminated in nearly the entire tensile elliptic regime except on the E, H boundary between r_2 and r_4. Thus, compressive lateral stress delays the appearance of both long and short wavelength limits of diffuse mode in the tensile regime ($s > 0$). And further increase in compressive lateral stress may suppress all short wavelength diffuse modes in the tensile elliptic regime. On the compressive side ($s < 0$), the E H boundary (in the softening range) between r_1 and r_3 expands as curve B moves downwards faster than curve A. However, the response diagram is quite similar to that of Fig. 8. Again, according to Fig. 3(d), compressive lateral stress enhances pre-peak diffuse mode with finite wave number. Hence, according to our hypothesis, the inception of shear band localization is more likely to occur preceding peak applied stress under compressive lateral stress.

As mentioned in Section 5.1, due to the mathematical complexity involved, the exclusion of bifurcations in the elliptic regime is not obvious compared with the plane strain analysis given by Needleman (1979) and by Chau and Rudnicki (1990). However, the numerical results obtained in Section 6 for diffuse modes suggest that bifurcation is excluded for the portion of tensile EC subregime which is above curve A, the maximum load point.

The discussion for the response regime given in this section is based on the assumption that other material parameters vary slowly with deformation comparing to the instantaneous tangent modulus E. A more realistic and complete picture of the possible bifurcations requires a good knowledge of the evolution of all constitutive parameters with deformation and stress states.

8. CONCLUSION

We have extended the previous bifurcation analyses of axisymmetric cylinders by Hutchinson and Miles (1974), and by Miles and Nuwayhid (1985) to include transverse anisotropy and non-normality by employing Rudnicki's (1977) model. The bifurcation analysis considers both diffuse geometric and localized shear band modes. The effects of the introduction of non-normality and transverse anisotropy on diffuse modes are examined in detail. Emphasis is given to study the relationship between diffuse modes and shear band modes.

Although the significance of both transverse anisotropy and non-normality on the shear band mode has been considered by Rudnicki (1977), for the sake of completeness, we have re-examined them in more detail in Section 4. In particular, as concluded by Rudnicki (1977), both transverse anisotropy and non-normality enhance the possibilities of pre-peak localization under axisymmetric compression but extreme values for material parameters have to be used.

More importantly, the effect of constitutive parameters on EC diffuse modes is studied numerically in Section 6. In general, the introduction of both transverse anisotropy and non-normality lowers the eigenstress for diffuse modes in both tension and compression. Furthermore, compressive confining stress is found to decrease the eigenstress levels at bifurcation in compression but increase them in tension. That is, compressive confining stress enhances diffuse modes in compression but retards them in tension. For short wavelength surface undulation, both transverse anisotropy and compressive confining stress reduce the eigenstress required for pre-peak bifurcations. However, the in-plane compressibility promotes the occurrence of pre-peak surface rumpling modes under compression but retards them under tension.

In addition, the long wavelength mode is always the first available bifurcation under tension. Even for finite specimen size ($a/L \neq 0$), necking seems to be the earliest possible kind of bifurcation under tension. In compression, for typical cylindrical geometry of a/L ranging from 1/4 to 1/6, the most likely bifurcation modes are those with wave number, $k = 3$ or 4 instead of bulging mode ($k = 1$). The angle of shear band promoted by these diffuse modes coincides with the theoretical prediction by Section 4. This observation leads to the hypothesis that pre-peak strain localization observed in experiments is triggered by the EC diffuse modes.

Guided by plane strain analysis (Hill and Hutchinson, 1975; Needleman, 1979; Chau and Rudnicki, 1990) and by axisymmetric analysis (Rudnicki, 1977; Miles and Nuwayhid, 1985) we have extended the bifurcation analysis for compressible circular cylinders to include non-normality and transverse anisotropy. However, the possible link between diffuse and localized modes, suggested in Section 7, requires further study.

Acknowledgements—The author is grateful to Professor John W. Rudnicki for suggesting this research and for his helpful and crucial comments during the course of the study. This work was supported by National Science Foundation Grants No. MSM-8612876 and No. MSS-8915607 to Northwestern University.

REFERENCES

Abramowitz, M. and Stegun, I. A. (Eds.) (1964). *Handbook of Mathematical Functions*, Appl. Math. Ser. 55, National Bureau of Standards, Washington, DC. (reprinted by Dover, 1965).

Bassani, J. L., Durban, D. and Hutchinson, J. W. (1980). Bifurcations at a spherical hole in an infinite elastoplastic medium. *Math. Proc. Camb. Phil. Soc.* **87**, 339–356.

Biot, M. A. (1965). *Mechanics of Incremental Deformations*. Wiley, New York.

Brace, W. F. (1964). Brittle fracture of rocks. In *State of Stress in the Earth's Crust* (Edited by W. R. Judd), pp. 111–174. Elsevier, Amsterdam.

Brace, W. F., Paulding, B. W. and Scholz, C. (1966). Dilatancy in the fracture of crystalline rocks. *J. Geophys. Res.* **71**, 3939–3953.

Chau, K. T. and Rudnicki, J. W. (1990). Bifurcations of compressible pressure-sensitive materials in plane strain tension and compression. *J. Mech. Phys. Solids* **38**, 875–898.

Cheng, S. Y., Ariaratnam, S. T. and Dubey, R. N. (1971). Axisymmetric bifurcation in an elastic–plastic cylinder under axial load and lateral hydrostatic pressure. *Quart. Appl. Math.* **29**, 41–51.

Elliott, H. A. (1948). Three-dimensional stress distributions in hexagonal aeolotropic crystals. *Math. Proc. Camb. Phil. Soc.* **44**, 522–533.

Fredrich, J., Evans, B. and Wong, T.-F. (1989). Micromechanics of the brittle to plastic transition in Carrara marble. *J. Geophys. Res.* **94**, 4129–4145.

Hadley, K. (1975). Azimuthal variation of dilatancy. *J. Geophys. Res.* **80**, 4845–4850.

Hill, R. (1958). A general theory of uniqueness and stability in elastic–plastic solids. *J. Mech. Phys. Solids* **6**, 236–249.

Hill, R. (1961a). Bifurcation and uniqueness in non-linear mechanics of continua. In *Problems of Continuum Mechanics*, contributions in Honor of the Seventieth Birthday of Academician N. I. Muskhelishvili, 16th February 1961 (Edited by M. A. Lavrent'ev *et al.*; English edition edited by J. R. M. Radok), pp. 155–164. Society for Industrial and Applied Mathematics, Philadelphia, PA.

Hill, R. (1961b). Discontinuity relations in mechanics of solids. In *Progress in Solid Mechanics* (Edited by I. N. Sneddon and R. Hill), Vol. 2, pp. 246–276. North-Holland, Amsterdam.

Hill, R. (1962). Acceleration waves in solids. *J. Mech. Phys. Solids* **10**, 1–16.

Hill, R. (1967). The essential structure of constitutive laws for metal composites and polycrystals. *J. Mech. Phys. Solids* **15**, 79–95.

Hill, R. (1968). On constitutive inequalities for simple materials—I. *J. Mech. Phys. Solids* **16**, 229–242.

Hill, R. (1978). Aspects of invariance in solid mechanics. In *Advances in Applied Mechanics* (Edited by C.-S. Yih), Vol. 18, pp. 1–75.

Hill, R. (1979). On the theory of plane strain in finitely deformed compressible materials. *Math. Proc. Camb. Phil. Soc.* **86**, 161–178.

Hill, R. (1983). Interfacial operators in the mechanics of composite media. *J. Mech. Phys. Solids* **31**, 347–357.

Hill, R. and Hutchinson, J. W. (1975). Bifurcation phenomena in the plane tension test. *J. Mech. Phys. Solids* **23**, 239–264.

Hutchinson, J. W. (1970). Elastic–plastic behavior of polycrystalline metals and composites. *Proc. Roy. Soc. Lond. A*, **319**, 247–272.

Hutchinson, J. W. and Miles, J. P. (1974). Bifurcation analysis of the onset of necking in an elastic/plastic cylinder under uniaxial tension. *J. Mech. Phys. Solids* **22**, 61–71.

Lin, T. H. (1971). Physical theory of plasticity. In *Advances in Applied Mechanics* (Edited by C.-S. Yih), Vol. 11, pp. 255–311.

Love, A. E. H. (1927). *A Treatise on the Mathematical Theory of Elasticity*. 4th Edn. Cambridge University Press (reprinted by Dover, 1944).

Miles, J. P. (1971). Bifurcation in plastic flow under uniaxial tension. *J. Mech. Phys. Solids* **19**, 89–102.

Miles, J. P. and Nuwayhid, U. A. (1985). Bifurcation in compressible elastic/plastic cylinders under uniaxial tension. *Appl. Sci. Res.* **42**, 33–54.

Mogi, K. (1967). Effect of the intermediate principal stress on rock failure. *J. Geophys. Res.* **72**, 5117–5131.

Needleman, A. (1979). Non-normality and bifurcation in plane strain tension and compression. *J. Mech. Phys. Solids* **27**, 231–254.

Prager, W. (1961). *Introduction to the Mechanics of Continua*. Ginn and Company, Boston (reprinted by Dover, 1973).

Press, W. H., Flannery, B. P., Teukolsky, S. A. and Vetterling, W. T. (1989). *Numerical Recipes: The Art of Scientific Computing*. Cambridge University Press, New York.

Raniecki, B. and Bruhns, O. T. (1981). Bounds to bifurcation stresses in solids with non-associated plastic flow law at finite strain. *J. Mech. Phys. Solids* **29**, 153–172.

Rice, J. R. (1976). The localization plastic deformation. In *Proc. 14th Int. Cong. Theoretical and Appl. Mech.* Delft (Edited by W. T. Koiter), Vol. 1, pp. 207–220, North-Holland, Amsterdam.

Rudnicki, J. W. (1977). The effect of stress-induced anisotropy on a model of brittle rock failure as localization of deformation. *Energy Resources and Excavation Technology, Proc. 18th U.S. Symposium on Rock Mechanics*, Keystone, Colorado, June 22–24, 1977, pp. 3B4-1–3B4-8.

Rudnicki, J. W. and Rice, J. R. (1975). Conditions for the localization of deformation in pressure-sensitive dilatant materials. *J. Mech. Phys. Solids* **23**, 371–394.

Rummel, F. and Fairhurst, C. (1970). Determination of the post-failure behavior of brittle rock using a servo-controlled testing machine. *Rock Mech.* **2**, 189–204.

Santarelli, F. J. and Brown, E. T. (1989). Failure of three sedimentary rocks in triaxial and hollow cylinder compression tests. *Int. J. Rock Mech. Min. Sci. & Geomech. Abstr.* **26**, 401–413.

Scholz, C. H. (1968). Experimental study of the fracturing process in brittle rock. *J. Geophys. Res.* **73**, 1447–1454.

Tvergaard, V., Needleman, A. and Lo, K. K. (1981). Flow localization in the plane strain tensile test. *J. Mech. Phys. Solids* **29**, 115–142.

Vardoulakis, I. (1983). Rigid granular plasticity model and bifurcation in the triaxial test. *Acta Mechanica* **49**, 57–79.

Wawersik, W. R. and Brace, W. F. (1971). Post failure behavior of a granite and a diabase. *Rock Mech.* **3**, 61–85.

Wawersik, W. R. and Fairhurst, C. (1970). A study of brittle rock fracture in laboratory compression experiments. *Int. J. Rock Mech. Min. Sci.* **7**, 561–575.

Young, N. J. B. (1976). Bifurcation phenomena in the plane compression test. *J. Mech. Phys. Solids* **24**, 77–91.